Journal of the Mechanics and Physics of Solids 74 (2015) 38–48

Contents lists available at ScienceDirect

Journal of the Mechanics and Physics of Solids

journal homepage: www.elsevier.com/locate/jmps

Morphology and dynamics of a crack front propagating in a model disordered material

J. Chopin [a,*], A. Boudaoud [b], M. Adda-Bedia [c]

[a] Civil Engineering Department, COPPE, Universidade Federal do Rio de Janeiro, 21941-972, Rio de Janeiro RJ, Brazil
[b] RDP, ENS Lyon, 46 allée d'Italie, 69007 Lyon, France
[c] Laboratoire de Physique Statistique, Ecole Normale Supérieure, UPMC Paris 6, Université Paris Diderot, CNRS - 24 rue Lhomond, 75005 Paris, France

ARTICLE INFO

Article history:
Received 17 September 2013
Received in revised form
10 February 2014
Accepted 10 June 2014
Available online 30 October 2014

Keywords:
Fracture
Coplanar propagation
Heterogeneous materials
Statistics
Adhesion enhancement

ABSTRACT

We present an experiment on the morphology and dynamics of a crack front propagating at the interface between an elastomer and a glass slide patterned with a prescribed distribution of defects. Regimes of high and low pinning strength are explored by changing the fracture energy contrast of the defects. We first analyze the roughness of crack fronts by measuring their typical amplitude in real and Fourier space. Irrespective of the pinning regime, no well defined self-affine behavior is found which may be explained by the emergence of an intermediate lengthscale between the defect size and the sample size. Then, we show that the dynamics at high fracture energy contrast results in rapid jumps alternating with periods of arrest. The distributions of speeds, displacements and waiting times are found to have an exponential decay which is directly related to the distribution of distances between defects along the direction of propagation.

1. Introduction

Due to progress in micro fabrication, microstructure of materials can be tailored to achieve unprecedented macroscopic properties such as negative Poisson ratio (Yang et al., 2004), superhydrophobicity and omniphobicity (Bonn et al., 2009), reversible and strong adhesion (Geim et al., 2003; Chan et al., 2007; Xia et al., 2012) and anti-biofouling property (Epstein et al., 2012). Regarding the mechanical properties, the addition of particles is well known to enhance mechanical properties, like in adobe, particles-loaded rubber (Mower and Argon, 1995), or nanosheets made of clay-reinforced composites (Alexandre and Dubois, 2000). Although remarkable achievements have been made over the past decade, it is still poorly understood how large-scale mechanical properties are linked to characteristics of the microstructure such as size and distribution of heterogeneities, or strength of bonding of heterogeneities and surrounding matrix. This link is crucial to predict and optimize the mechanical stability of multilayered composite materials or, in the context of safety, the service lifetime of engineering structures.

Fractography is one of the most useful tools to determine the cause and dynamics of failure of a material. It relies on a visual inspection of the postmortem cracked surfaces (Hull, 1999). Some morphological features are specific to modes of failure such as periodic strips in fatigue crack (Suresh, 1998) or facets for brittle crack (Lawn, 1993). A morphological feature

* Corresponding author.
E-mail address: jchopin@clarku.edu (J. Chopin).

http://dx.doi.org/10.1016/j.jmps.2014.10.001
0022-5096/

found in heterogeneous material is the fractal (or self-affine) geometry of broken surfaces. Since the seminal work by Mandelbrot et al. (1984), numerous experimental characterizations with a wide range of materials and fracture protocols have been carried out to check the scale invariance and to measure associated roughness exponents (Bouchaud et al., 1990; Engoy et al., 1994; Plouraboué et al., 1996; Ponson, 2007; Dalmas, 2008). This specific morphology has been interpreted as the result of a critical dynamics during the crack propagation through the heterogeneous material (Bouchaud, 1997; Bonamy, 2008, 2009).

To the best of our knowledge only one experimental setup developed by Schmittbuhl and Måløy enables testing this interpretation by the direct visualization of the crack front dynamics (Schmittbuhl and Måløy, 1997). In this setup, a crack front propagates at the interface of two sintered Plexiglas plates. Before sintering, the plates are sandblasted to induce a disorder with a typical size given by the diameter of projected beads. Using a subtle statistical analysis, they obtained information on the shape and the dynamics of the crack front (Delaplace, 1999; Santucci et al., 2010). For scales larger than the typical size of heterogeneities, they found that crack propagation is well described by models first introduced by Gao and Rice (1989), and improved later on Schmittbuhl et al. (1995). Critical exponents characterizing the morphology (roughness exponent) and dynamics (scale-free avalanches) are found to agree with theoretical predictions (Bonamy, 2008, 2009). However, at smaller scale, the crack propagation is explained by another scenario based on growth by coalescence of microcracks which accounts for the unexpectedly high roughness exponent at that scale (~ 0.6). While the interpretation of their experimental results brings a coherent picture of the crack front dynamics in their setup, some aspects need to be clarified. First, there is no clear experimental evidence of a diffuse front moving by microcracks coalescence at small scale. Second, the lengthscale separating the roughness regime is located in the middle of the observation window and, thus, prevents a clear identification of both roughness regimes over a large range of lengthscales. Therefore, a better understanding of the rupture process at the microstructure scale and a better control of the disorder are needed. Along these lines, other setups have been developed to enable a better control of deterministic heterogeneities using lithographic techniques (Chopin et al., 2011) or micro-machined interfaces (Dalmas et al., 2009), and experimental results were often in quantitative agreement with models developed within the framework of Linear Elastic Fracture Mechanics (LEFM). However, the case of a completely disordered interface has not been considered yet with these approaches.

In this paper, we present an original experimental setup where the shape and dynamics of a crack front are analyzed while propagating through an interface patterned with a prescribed random distribution of defects. We address the influence of the distribution of defects on the front shape and dynamics. Our experimental results will be interpreted in the framework of LEFM for which dissipative processes are assumed to be localized in a small region around the crack tip (the process zone) and are traditionally characterized by a fracture energy Γ. The crack front will propagate if the loading is high enough to overcome the energetic cost to create a new interface which happens when $G > \Gamma$, where G is the elastic energy release rate, i.e. the elastic energy released during fracture per unit of newly created fracture surface area. Consequently, the crack is at equilibrium when $G = \Gamma$. When a material is heterogeneous because of, for example, voids or inclusions, the fracture energy presents spatial fluctuations that are responsible for the distortion of crack front shape. For moderate fracture energy contrast, the crack front is slightly distorted at the defect scale and is then amenable to perturbative approaches (Gao and Rice, 1989). In this regime, the crack front can be understood as an elastic line with a nonlocal elasticity forced by a quenched noise (see Kardar, 1998, for a review). It was found that at small scale, the crack front presents smooth deformations and continuous dynamics. Above a crossover which depends on the system size and on the characteristics of the disorder, numerical and theoretical results show that the crack front shape has scale invariant properties with self-affine behavior (Roux et al., 2003; Patinet et al., 2013; Démery, 2014). Moreover, the crack propagates intermittently through avalanches which consist of rapid events where a part of the front moves from one pinned configuration to another. This regime at large scale has been studied intensively but no clear agreement of the predicted roughness exponent with experimental data has been obtained so far (Schmittbuhl and Måløy, 1997; Delaplace, 1999; Santucci et al., 2010). Many reasons have been proposed to explain this disagreement: the influence of nonlinear terms in the elastic energy release rate (Adda-Bedia et al., 2006), finite size effects (Katzav et al., 2007; Leblond, 2003; Patinet et al., 2013), artifacts in the analysis of experimental data (Schmittbuhl et al., 1995; Bakke and Hansen, 2007), or more fundamentally the questioning of the validity of LEFM approach (Hansen and Schmittbuhl, 2003).

The paper is organized as follows. In Section 2, we describe the experimental setup, the fabrication of the sample using lithographic techniques, the method of visualization and extraction of the crack front shape over time. Two regimes of pinning strengths are explored by changing the fracture energy contrast from a high to a low value. In Section 3, we analyze the roughness of the crack front shape using statistical tools. In either regimes, the fluctuations do not show scale invariant behavior over significant ranges of lengthscales. This result is explained by the emergence of an intermediate lengthscale which is the geometrical mean of the defect size and the size of the sample. This lengthscale is derived by calculating the shape of crack front pinned by a single defect taking into account a finite crack length. In Section 4, we analyze the statistics of front dynamics by calculating the distributions of speed and displacement in both regimes. For high fracture energy contrast, we find that the crack dynamics is slaved to the distribution of defects through the distance between pinning points.

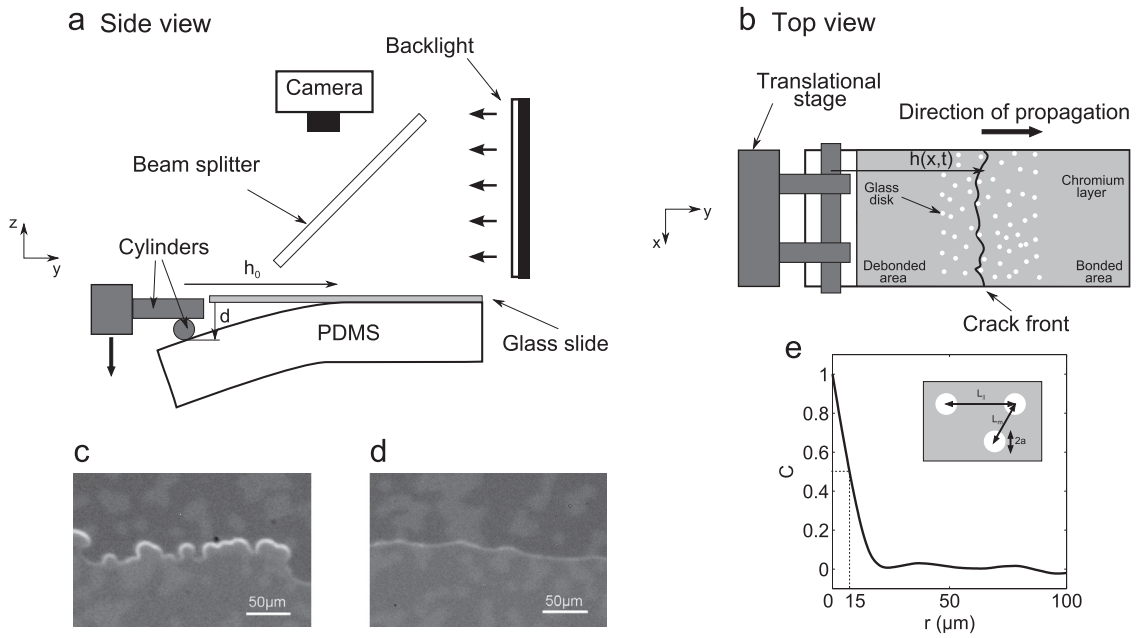

Fig. 1. Experimental setup. (a) Schematic side view. A silicon elastomer is peeled from a patterned glass substrate by means of a translating stage imposing a deflection d. (b) Schematic top view. The substrate can be made chemically heterogeneous. (c) and (d) Pictures of the front (bright line) using a binocular for a high (c) and low (d) fracture energy contrast $\delta\Gamma/\Gamma_0$. (e) Normalized cross correlation of the disorder with $\eta = 35\%$ showing a short range correlation of 15 μm which corresponds to the defect diameter. Inset : Definition of the parameters that rule the distribution of defects (white disks of diameter $2a$). L_m is the mean distance between defects and $L_\parallel$ is the mean distance between defects along the direction of crack propagation (y-axis).

2. Experimental setup

In this experiment, a silicon elastomer in contact with a glass substrate is peeled using the configuration of a beam cantilever. The elastomer is a crosslinked polydimethylsiloxane (PDMS, Sylgard184, Dow Corning) of Young's modulus $E \simeq 2$ MPa prepared following a standard protocol (Chopin et al., 2011). The samples are 10 mm thick, 76 mm long and 22 mm large, the two latter dimensions being imposed by the use of microscope slides (dimensions 25×76 mm) as a substrate. The glass slides are clamped on an aluminum frame. A deflection d of the elastomer beam is imposed using two cylinders rigidly attached to a piezo-electric translation stage (NanoPZ, Newport) (Fig. 1). An additional cylinder is glued to the elastomer using PDMS, thus providing two cross-cylinder contacts with no tension induced and minimal friction. The crack front corresponds to the boundary between bonded and debonded regions (Fig. 1(a))

Pictures are taken using a digital camera (Nikon, D300) mounted on a binocular (MZ16, Leica) which is equipped with a LED ring for illumination. The CCD sensor of the camera has 3872×2576 pixels, one pixel is 4 μm. The illumination makes the front appear as a bright line and the defects as lighter gray areas (Fig. 1(c) and (d)). When a picture of the front over a wider range of lengthscales is needed, we use a macro objective (Nikon) so that one pixel has a side length of 15 μm; the sample is then lit using a beamsplitter and a backlight (Phlox, Stemmer Imaging) placed vertically on the side, so that the front corresponds to a boundary between two gray levels. Pictures are taken every 10 s. By adjusting the deflection rate with the stepper motor, the mean speed of the crack front v_m is kept constant, of the order of 0.1 μm/s. The crack front shape is determined using a home-made algorithm detecting maximal contrasts, and yielding the front position $h(x, t)$ at a subpixel resolution. The mean position of the front is defined as the spatial average of h along the transverse direction x, $h_0(t) = \langle h(x, t)\rangle_x$.

The glass substrate can be made chemically heterogeneous enabling the spatial modulation of the fracture energy Γ of the interface. Using standard soft lithography techniques (Chopin et al., 2011), a nanometric chromium layer is deposited in prescribed areas of the glass slide. PDMS adheres more strongly to glass than to chromium. The glass plate is patterned by a random distribution of defects which are disc-shaped areas of radius a devoid of a chromium coating (Fig. 1(b)). Defects of arbitrary shape, size and spatial distribution can be printed with a minimal size of 20 μm over an area of 20 mm^2 (Fig. 1 (c) and (d)). The x and y coordinates of each disk are obtained using a random number generator with a uniform distribution where overlap is allowed. The spatial distribution of the discs is uncorrelated for distances larger than $2a$ (see Fig. 1(e)). The fracture energies of homogeneous PDMS-glass Γ_G and PDMS-chromium Γ_0 are measured (Chopin et al., 2011) and are found to be $\Gamma_G \sim 7\text{J}\cdot\text{m}^{-2}$ and $\Gamma_0 \sim 0.1\text{J}\cdot\text{m}^{-2}$. An adhesive strip of width 200 μm (devoid of chromium) is printed before the disordered area which allows us a direct in situ estimation of $\delta\Gamma/\Gamma_0$ by measuring the aspect ratio of the crack front tip when sweeping the strip (Chopin et al., 2011). In Fig. 1(c–d), we show two examples of crack fronts in a disordered interface. In Fig. 1(c), when peeling the PDMS block for the first time, the crack front (bright line) can exhibit overhangs and even

Table 1
Characteristic parameters of the distribution of defects and working parameters for Exp. 1, 2, and 3. The defects are disks of radius $a \sim 10\,\mu m$. η is the density, $L_m \sim a/\sqrt{\eta}$ the mean distance between defects, and $L_\parallel \sim a/\eta$ the mean distance between defects along the direction of propagation. v_m is the mean velocity of the front and $\delta\Gamma/\Gamma_0$ the fracture energy contrast where $\delta\Gamma = \Gamma_G - \Gamma_0$, Γ_G and Γ_0 the glass and chromium fracture energy respectively.

Exp.	η (%)	2a (μm)	L_m (μm)	$L_\parallel$(μm)	v_m (μm/s)	$\frac{\delta\Gamma}{\Gamma_0}$
1	20	18	44	58	0.15	10–14
2	35	15	26	55	0.30	10–14
3	35	18	44	58	0.14	1

filaments due to a high fracture energy contrast ($\delta\Gamma/\Gamma_0 \sim 10$–14) and move according to an intermittent dynamics. The fracture energy contrast can be lowered to $\delta\Gamma/\Gamma_0 \sim 1$ after subsequent cycles of bonding-peeling (Fig. 1(d)). In the vicinity of the strip, models based on perturbative approach are not valid because the slope of the crack front is large. However, it was shown that they remain valid far enough from the strip. We found that the slope rapidly decays and reaches value below 1 at a distance *2a* from the strip.

The distribution of defects can be characterized using three parameters: the density η, the mean distance between defects L_m and the mean distance $L_\parallel$ between defects along the *y*-axis (along the direction of the crack propagation, see Fig. 1 (e), inset). The density of defects is defined as the area covered by the defects over the area of the patterned surface. It is noteworthy that the procedure of substrate patterning yields a Poisson distribution, $P(l_\parallel) = 1/L_\parallel \ \exp(-l_\parallel/L_\parallel)$, for the distance $l_\parallel$ between defects along the *y*-axis. These parameters are given in Table 1, along with the mean velocity of the front and an estimation of the fracture energy contrast.

3. Crack front morphology

In Fig. 2, we show a crack front from Exp. 1 after image processing. The shape results from two contributions: defect induced fluctuations at small scale and a parabolic-like trend at large scale which is exaggerated by the scale difference in the *x* and *y* axes. This trend which is due to an anticlastic effect can be estimated by a quadratic fit (dotted line in Fig. 1(a)). The typical radius of curvature of the parabola (~ 0.5 m) is larger than all other lengthscales but affects dramatically the statistical analysis of the profile. The whole front is corrected by subtracting the fitted shape from the actual front and, to simplify notations, the profile is noted $h(x, t)$. Fig. 2(b) shows a corrected crack front along with a magnified part of length Δx illustrating that the fluctuations can be observed over a wide range of lengthscales.

The amplitude of the corrected crack front is now analyzed using the Height-Height Correlation (HHC) method and Power Spectrum analysis (PS). In the HHC method, the amplitude σ of the fluctuations is evaluated within a band of width Δx starting at x (see Fig. 2(b), inset) and averaged over all possible origins x and all fronts (all values of time t):

$$\sigma(\Delta x) = \sqrt{\langle (h(x + \Delta x, t) - h(x, t))^2 \rangle_{x,t}} \tag{1}$$

Fig. 2(c) shows the evolution of σ with Δx for Exp. 1, 2 and 3. As expected, the amplitude of the fluctuations increases when evaluating over increasing lengthscales. Lines corresponding to roughness exponents $\zeta = 0.25$ and 0.85 are shown as guides for the eyes. σ is observed to have the same tendency for Exp. 1 and 2 whereas for Exp. 3, σ is smaller which reflects a smaller fracture energy contrast. We emphasize that no well-defined roughness exponent is observed over the observation window, instead the data show two crossovers l_c and L_c (vertical lines). The lengthscale l_c is interpreted as a cutoff related to the defect size and is found to be 35 μm for Exp. 1 and 2 and 100 μm for Exp. 3. When $\Delta x < l_c$, the roughness is 0.8 which is consistent with the roughness of a smooth front with positive correlations (see Fig. 1(d)). When $\Delta x > L_c$, the roughness is approaching zero which is what one would expect for a flat horizontal profile at large scale. For small fracture energy contrast, l_c is found to be larger which can be interpreted by the fact that weaker defects would significantly distort the front at larger lengthscale therefore extending the regime of high roughness exponent. However, L_c is found to remain roughly unchanged underlying a different physical origin such as boundary effects.

To obtain further insight into the statistics of fluctuations, we measure the power spectrum (PS) of corrected fronts which is estimated by calculating the periodogram $S(\lambda)$ of h:

$$S(\lambda) = \frac{1}{2L}\left|\sum_{x=1}^{2L} h(x) e^{-i2\pi x/\lambda}\right|^2, \quad \lambda = 2, 3, \ldots, L \tag{2}$$

A Hanning window is also used to reduce spurious contributions due to the finite length of the front. In Fig. 2(d), the PS for all experiments is plotted as a function of the wavelength λ. We find that a regime of rapid increase of the amplitude of fluctuations for $\lambda \sim l_c$ is followed by a regime of slower evolution at larger λ. The transition between the two regimes l_c depends on the experiments and is less sharp when the fracture energy contrast is lowered. As a guide for the eyes, power law of exponent 1.5 is shown which corresponds to a roughness exponent $\zeta = 0.25$. Overall, the fluctuations of the front

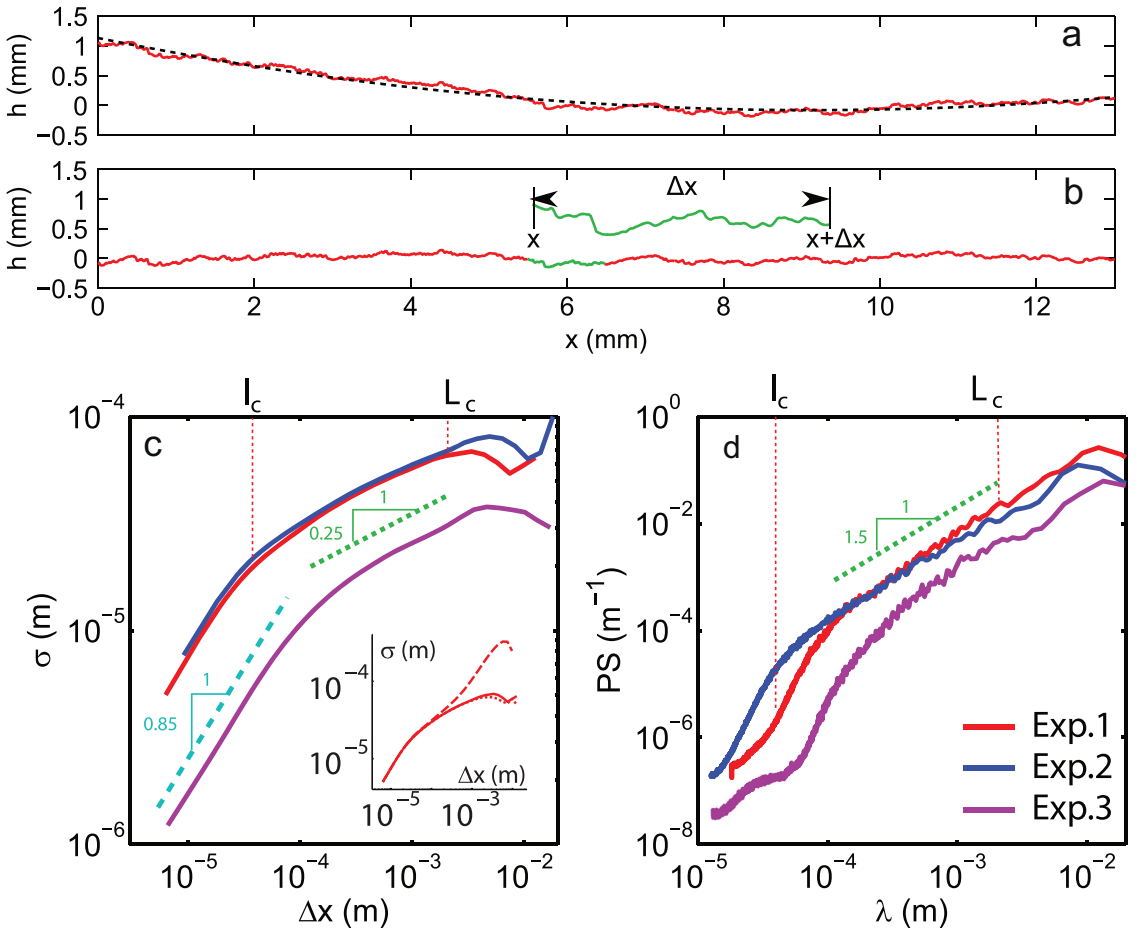

Fig. 2. Spatial analysis of crack fronts. (a) Crack front shape (solid red line) from Exp. 1 obtained after image processing. Note that the two axes have different scales. The large scale trend is estimated by a fit with a quadratic polynomial (dashed line). (b) Corrected front after subtraction of the trend. Inset : Part of the front (green line) of length Δx starting at x showing fluctuations at smaller length scale. (c) Standard deviation of the corrected front as a function of window length Δx for Exp. 1, 2, and 3 using the Heigth–Height correlation (HHC) method. Power laws with exponent 0.85 (blue dashed line) and 0.25 (green dotted line) are shown. The small and large scale crossovers, l_c and L_c respectively, are shown. Inset : σ for Exp. 1 calculated after using linear (dashed line), quadratic (solid line) and cubic (dotted line) corrections. σ is largely overestimated at large scale when using a linear correction. (d) Power spectrum of the corrected front as a function of λ. A Hanning window is also used to reduce spurious contributions due to the finite length of the front. Power law with exponent 1.5 (green dotted line) is shown. (For interpretation of the references to color in this figure caption, the reader is referred to the web version of this paper.)

increase with the fracture energy contrast $\delta\Gamma/\Gamma_0$. Indeed, at larger fracture energy contrast, the disorder induces more distortion to the crack front while the elastic restoring force remains unchanged. The typical size for these fluctuations is $a\delta\Gamma/\Gamma_0$ where a is the defect characteristic size. Surprisingly enough, the transition from high to low fracture energy contrast is not reflected by a qualitative change in roughness curves shown in Fig. 2.

Following Schmittbuhl et al. (1995), we verified that our statistical analysis is not biased due to discontinuities in the signal, finite size effects or global trends. In particular, we checked that no change in the roughness curves is observed when correcting the crack profile with polynomials of higher order as shown in the inset of Fig. 2(c). However, the results from the two analyses (HHC and PS) do not provide unambiguous results for the existence of self-affine profiles with well-defined roughness exponents. This can be attributed to the existence of a crossover at approximately 1 mm which is responsible for an absence of self-affinity of the crack front. This crossover is rather surprising because it is smaller than the system size ($\sim$ 20 mm) and larger than the defect size ($\sim$ 0.02 mm). This is in contrast with the experiment of Schmittbuhl and Måløy (1997) on a similar system where they found two different roughness exponents for lengthscales smaller and larger than the typical size of disorder. However, we note that in our experiment, the amplitude of fluctuations is always measured at scales larger the defect size.

In the following, we argue for the existence of a new lengthscale that is intermediate between defect size and sample size. The theoretical interpretation of crack front dynamics in disordered materials has often been based on the formula that provides the first-order variation of the stress intensity factor resulting from some small, but otherwise arbitrary coplanar perturbation of the front of a semi-infinite crack in an infinite body (Gao and Rice, 1989). To be applicable to experiments,

this requires that the characteristic distance of variation of this perturbation in the direction of the crack front be small compared to all other dimensions of the problem. In Legrand et al. (2011), the variation of the local mode I stress intensity factor for a cantilever crack that takes into account the cracked geometry and boundary conditions used in experiments has been provided. In order to apply the latter results to our experimental situation within a tractable model, several approximations should be made. First, we neglect the effect of the mode mixing induced by the asymmetric beam cantilever geometry of the experimental setup. Second, the dependence of the toughness with the local speed of the front is neglected because the crack front propagates at velocity $v_m \sim 0.1$ μm/s smaller that the characteristic velocity of dissipative processes $c \sim 20$ μm/s (Chopin et al., 2011). Third, we address the effect of a single finite geometrical length scale, namely the situation of a planar crack of length h_0 lying on the mid-plane of a very thin plate. This is not the case of the present experimental situation, where the thickness of the sample is finite and can also be a screening length for the crack front fluctuations. However, this limit allows analytic results that illustrate the effect of finite geometry of the sample on the crack front shape. We will discuss in the following the general validity of this approximation when the thickness of the sample is taken into account.

We consider the situation of a sample in which a planar crack front is pinned by a single defect consisting of an adhesive strip, the rest of the interface being homogeneous. The strip is then modeled by a spatially modulated fracture energy

$$\Gamma(x) = \Gamma_0 + \delta\Gamma(x) \tag{3}$$

where $\delta\Gamma(x)$ is a rectangular gate function of width $2a$:

$$\delta\Gamma(x) = \begin{cases} \delta\Gamma & \text{if } |x| < a, \\ 0 & \text{if } |x| > a \,, \end{cases} \tag{4}$$

with $\delta\Gamma \ll \Gamma_0$. When there is no adhesive strip, the crack length, the elastic energy release rate and the fracture energy are noted h_0, G_0 and Γ_0 respectively. The strip induces perturbations $\delta h(x)$ and $\delta G[x, \delta h]$ of the front shape and the elastic energy release rate respectively. Under the assumption of small slope $|h'(x)| \ll 1$, $\delta G[x, \delta h]$ is given by Legrand et al. (2011)

$$\frac{\delta G}{G_0} = 2PV \int_{-\infty}^{+\infty} f\left(\frac{x' - x}{h_0}\right) \frac{\delta h(x') - \delta h(x)}{(x' - x)^2} \frac{dx'}{2\pi} \tag{5}$$

where PV stands for the Principal Value of the integral and $f(u)$ is a weight function. In the Fourier space, Eq. (5) simplifies into

$$\frac{\widetilde{\delta G}(q)}{G_0} = 2F(qh_0) \frac{\widetilde{\delta h}(q)}{h_0} \tag{6}$$

with Legrand et al. (2011)

$$F(p) = \frac{2p\cosh(2p) - \sinh(2p)}{2p - \sinh(2p)}. \tag{7}$$

Using the Griffith criterion one can relate the spatially modulated fracture energy to the crack front shape through

$$\frac{\delta\Gamma(x)}{\Gamma_0} = \frac{\delta G(x)}{G_0} \tag{8}$$

Here, the zeroth order solution $\Gamma_0 = G_0$ has been used. Using the expression (4) for the fracture energy contrast, the expression of the front shape in the Fourier space is given by

$$\frac{\widetilde{\delta h}(q)}{h_0} = \frac{\delta\Gamma}{\Gamma_0} \frac{\sin qa}{qF(qh_0)} \tag{9}$$

and in the real space the solution reads

$$\frac{\delta h(x)}{h_0} = \frac{1}{2\pi} \frac{\delta\Gamma}{\Gamma_0} \int_{-\infty}^{+\infty} \frac{\sin qa}{qF(qh_0)} e^{iqx}\, dq \tag{10}$$

This integral does not admit an analytic expression. In order to look for the asymptotic behavior of $h(x)$ near defect and far from defect, it is useful to replace $F(p)$ by an approximate form $F_0(p)$ given by

$$F_0(p) = -2\sqrt{1 + p^2} \tag{11}$$

The function $F_0(p)$ displays the same asymptotic behavior as $F(p)$, namely $F_0(0) = -2$ and $F_0(p) \approx -2|p|$ for large p. Moreover, the ratio $F(p)/F_0(p)$ is always close to unity showing that $F_0(p)$ is a good approximation for $F(p)$ for all p. Substituting in Eq.

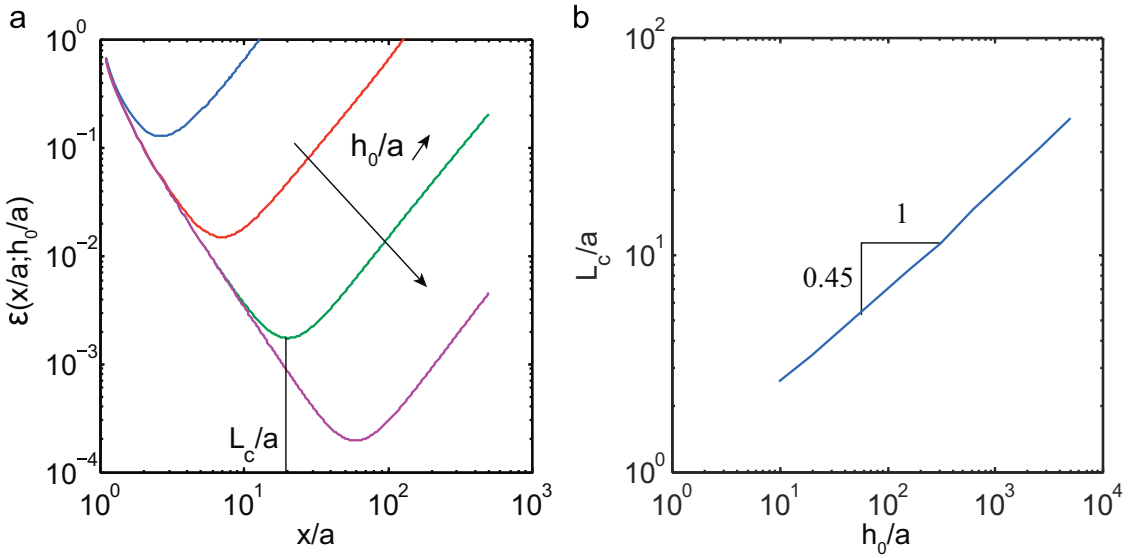

Fig. 3. (a) Ratio $\epsilon = |\delta h_{\dot{N}D}/\delta h_{\dot{F}D} - 1|$ as a function of x/a for $h_0/a = 10,\ 10^2,\ 10^3,\ 10^4$. The crossover length L_c/a is defined as the minimum of each curve. (b) The curve L_c/a as a function of h_0/a is best fitted by $A(h_0/a)^{\alpha}$ where $\alpha = 0.45$ and $A = 0.89$.

(10), one obtains

$$\delta h'(x) = -\frac{\delta\Gamma}{4\pi\Gamma_0}[K_0(|x+a|/h_0) - K_0(|x-a|/h_0)], \tag{12}$$

where K_0 is the modified Bessel function of zeroth order. Near defect, recognizing that $a \sim |x| \ll h_0$, Eq. (12) gives

$$\text{Near defect:}\quad \delta h_{\dot{N}D}(x) \approx \frac{\delta\Gamma}{4\pi\Gamma_0}\log\left|\frac{1+x/a}{1-x/a}\right|, \tag{13}$$

yielding after integration the front shape given in Chopin et al. (2011). Far from the defect ($|x| \gg a$), Eq. (12) gives

$$\text{Far from defect:}\quad \delta h_{\dot{F}D}(x) \approx \frac{\delta\Gamma}{2\pi\Gamma_0}(a/h_0)K_1(x/h_0), \tag{14}$$

where K_1 is the modified Bessel function of first order. The transition between the front slope near defect and far from defect occurs for a crossover lengthscale L_c. In order to estimate L_c, we introduce

$$\epsilon(x/a;\, h_0/a) = \left|\frac{\delta h_{\dot{N}D}}{\delta h_{\dot{F}D}} - 1\right|, \tag{15}$$

The function $\epsilon(x/a;\, h_0/a)$ is expected to reach a minimum at the crossover length $x = L_c$ when the solution near and far from defect are of the same order of magnitude ($\delta h_{\dot{N}D} \sim \delta h_{\dot{F}D}$). Indeed, Fig. 3(a) shows that $\epsilon(x/a;\, h_0/a)$ exhibits an absolute minimum which is found to increase with h_0/a. From a fit of the data (see Fig. 3(b)), we find that the crossover follows the scaling:

$$\frac{L_c}{a} = A\left(\frac{h_0}{a}\right)^{\alpha}, \tag{16}$$

with $A = 0.89$ and $\alpha = 0.45$. Therefore the large scale crossover L_c is found to be much smaller than any other macroscopic lengthscale. Indeed, recognizing that $\alpha \approx 1/2$, L_c is approximately the geometric mean of a microscopic quantity (the defect size) and a macroscopic quantity (the crack front length), thus, making any scale invariant regime difficult to probe experimentally.

This cutoff may have a significant influence on the interpretation of roughness analysis. Indeed, the self-affine properties of crack front rely exclusively on the logarithmic response from one defect or equivalently to the nonlocal elasticity. The large scale cutoff provides a natural screening length for the elastic interaction over which the amplitude of fluctuation starts to saturate. In our experiment, $L_c \sim 0.6$ mm, which is in the same order of magnitude than the crossover estimated experimentally and shown in Fig. 2(c) and (d). The analysis we developed illustrates how finite size effect reflects on the front elasticity based on a simplified model. The existence of a cutoff at an intermediate length scale is a robust result which persists when the full complexity of the system is taken into account. The presence of mode mixing or the finite thickness of sample will certainly affect the prefactor in Eq. (16) but it is unlikely that the exponent will be affected.

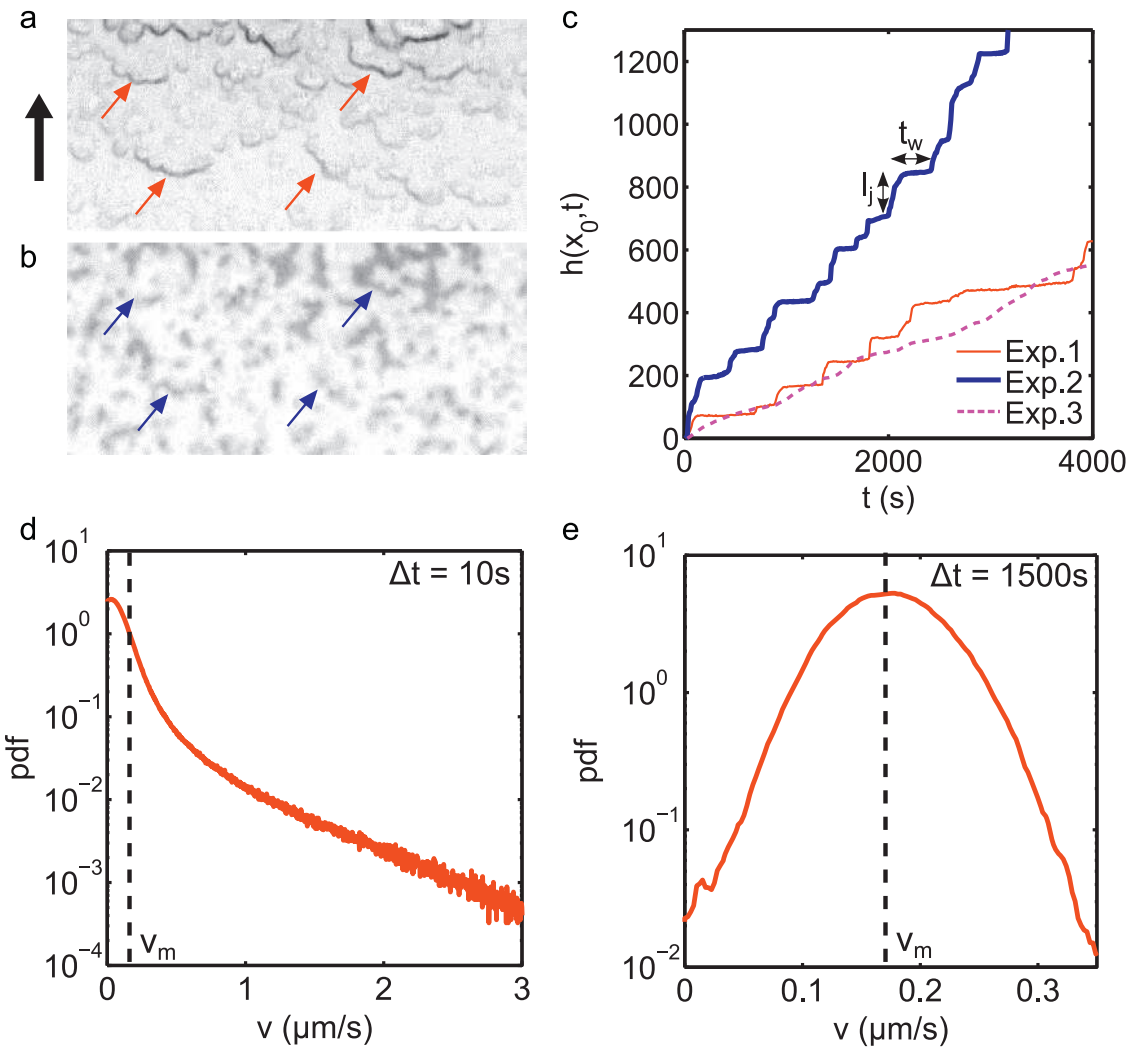

Fig. 4. Temporal analysis of crack fronts. (a) Superimposition of all pictures of the interface when the crack front has propagated from bottom to top (Exp. 1). The darker the region, the more time the front stopped (see red arrows). The picture width is ~1 mm (b) Corresponding picture of the defects (gray areas). The blue arrows drawn at the same locations as the red one roughly correspond to regions of high fracture energy. (c) Temporal evolution of $h(x_0, t)$ which corresponds to the evolution of one point of the front located at $x = x_0$ over time t for Exp. 1 (thin red line), Exp. 2 (thick blue line), and Exp. 3 (dashed magenta line). At high fracture energy contrast (Exp. 1 and Exp. 2), fast jumps of size l_j alternates with arrest periods of duration t_w. (d) Lin–log plot of the probability distribution function (pdf) of the speeds showing a peak at small velocity compared to the mean velocity v_m and an exponential tail for larger velocities. The speed is evaluated over a duration $\Delta = 10$ s. (e) Linear–logarithmic plot of the pdf of the velocities at longer time $\Delta = 1500$ s. When Δ is increased, the pdf converges to a Gaussian distribution with v_m as a mean. (For interpretation of the references to color in this figure caption, the reader is referred to the web version of this paper.)

Except for the intensity of the fracture energy contrast, the analysis of the crack front shapes does not change qualitatively with the three different types of disorder used. We show in the following that the statistics of the crack front dynamics reveals tight connections with the distributions of defects.

4. Crack front dynamics

In Fig. 4(a), we show superimposed pictures of the crack front while propagating in a disordered interface with a high fracture energy contrast. When a part of the crack front remains in the same location from one picture to the next one, the corresponding area in the picture becomes darker. Sharp and disconnected dark lines correspond to pinned positions (see blue arrows) and illustrate an intermittent dynamics characterized by crack arrests alternating with jumps. More interestingly, we can relate the pinned positions with the location of defects. In Fig. 4(b), the distributions of the defects swept by the front are shown. We can see that pinned parts of the front are located in regions of higher fracture energy (see red arrows).

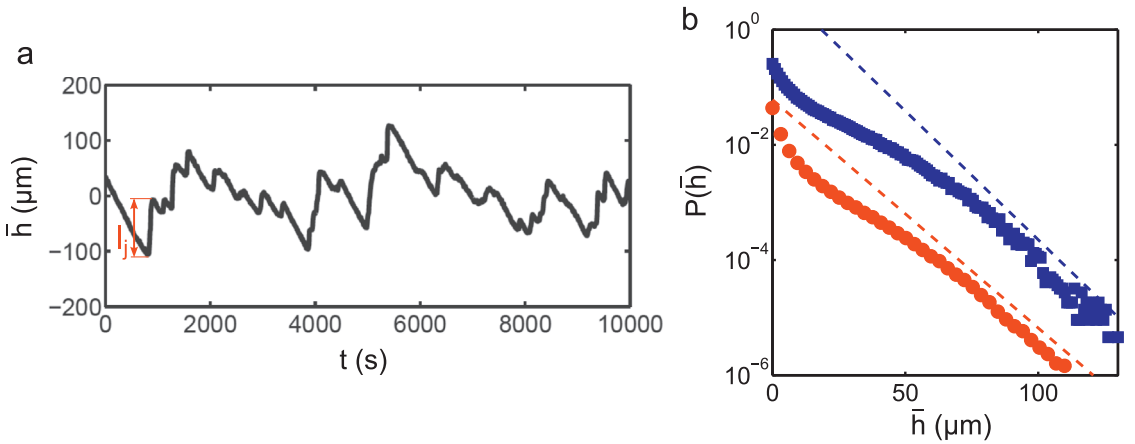

Fig. 5. Analysis of displacements at high fracture energy contrast. (a) Temporal evolution of the displacement $\bar{h} = h - v_m t$ relative to the mean front position for Exp. 1. (b) Pdf of forward displacements $\bar{h} > 0$ relative to crack front mean position for Exp. 1 ● and Exp. 2 ■. $\bar{h}$ is measured for a duration $\Delta t = 30$ s. Large displacements correspond to jumps which are distributed according to an exponential. Using a fit of the slope (dashed lines), characteristic jump sizes are estimated to be $L_j = 11$ μm for Exp. 1 and 10 μm for Exp. 2.

We now turn to a quantitative approach and we consider the temporal evolution $h(x_0, t)$ of one point of the crack front located at $x = x_0$. In Fig. 4(c), $h(x_0, t)$ is plotted as a function of time for Exp. 1 (see Table 1). Note that the initial position is set to 0 and that the total duration of the propagation is actually 10 times longer. The time series exhibits almost vertical lines corresponding to jumps alternating with plateaus corresponding to arrest periods. This features seem to disappear for Exp. 3 where the motion appears smoother.

In a first statistical analysis, we measure the speed $v(x_0, t) = [h(x_0, t + \Delta t) - h(x_0, t)]/\Delta t$ where Δt is the increment of time. In Fig. 4(d), we show the probability density function (pdf) of the speed for large Δt. The speed is observed to follow a Gaussian distribution with v_m as a mean. When Δt is much smaller and equal to the acquisition frame rate ($\Delta t = 10$ s), the pdf is qualitatively different, featuring a peak for $v \ll v_m$ and an exponential tail for $v \gg v_m$. The peak corresponds to arrest periods with a width given by the accuracy of speed measurements which is around ~0.1 μm/s. The large speeds correspond to jumps of the front from one area of high fracture energy to another. The observation of an exponential tail is in clear contrast with previous experiments where an algebraic decay of the pdf has been observed (Måløy and Schmittbuhl, 2001; Tallakstad et al., 2011). In order to understand the origin of the exponential behavior, we analyze the statistic of jumps and arrests periods. We focus on the case of strong pinning where the dynamics is discontinuous or intermittent and for which the following analysis is relevant.

We consider the displacements relative to the mean front position which are defined as $\bar{h}(x_0, t) = h(x_0, t) - v_m(x_0)t$ where v_m is obtained by a linear fit of $h(x_0, t)$. In Fig. 5(a), we plotted the temporal evolution of $\bar{h}(x_0, t)$ which shows steep ascending slopes corresponding to jumps of size l_j and weak descending slopes (about $-v_m$) corresponding to arrest periods. We focus our attention now on the statistics of jumps which coincide with the statistics of $\bar{h}$ when $v \gg v_m$. In Fig. 5(b), we show in a linear–logarithmic plot the pdf of the displacement for Exp. 1 and 2. Jumps larger than 50 μm are also distributed exponentially, $P(l_j) \sim \exp(-l_j/L_j)$. By an exponential fit of the tail, we extract the characteristic length scale for the jumps L_j, which is found to be 11 μm for Exp. 1 and 10 μm for Exp. 2 with only a weak dependence with the time interval Δt. Although v_m is two times smaller for Exp. 1 than for Exp. 2, it does not affect significantly L_j. This is an important qualitative result since a lengthscale is found in the local speed distribution unlike in the experiment reported in Santucci et al. (2010) where scale invariant features have been found. It is expected that this characteristic lengthscale L_j which is much smaller than the size of the specimen or even L_c is expressed as a combination of the defect size a and the density of defects η which are the only two parameters characterizing the statistics of the disorder. In the following, we argue that L_j scales as $L_\parallel \sim a/\eta$.

The origin of the exponential distribution of jumps with a characteristic length independent of v_m can be interpreted with the following argument. As shown in Fig. 4, the crack front is observed to move rapidly from a defect to the following one, it is then expected that the distribution of jumps follows the distribution of $l_\parallel$, the distance between two successive defects along the crack propagation. Therefore, the Poisson distribution of $l_\parallel$ should account for the origin of the exponential tail for the pdf of jumps. $L_\parallel$ for Exp. 1 and Exp. 2 is however larger (~ 50 μm) than L_j, which may be ascribed to the elasticity of the front that reduces jump sizes. At low fracture energy contrast (Exp. 3), the distribution is qualitatively different from Exp. 1 and Exp. 2 exhibiting no clear exponential nor algebraic decay (data not shown). In this case, although a regime of weak pinning can be expected, associated scale invariant properties are not well defined. Conversely, features of the high fracture energy contrast are local and, therefore, more easily probed. This strong relationship between the distribution of jumps at short time and the distribution of $l_\parallel$ was made using a given, yet generic, type of disorder obtained by a random, uncorrelated, deposition of disks. It will be of great interest to vary the disk diameter and, in a broader range, the density of defects and examine the limit of validity of our results.

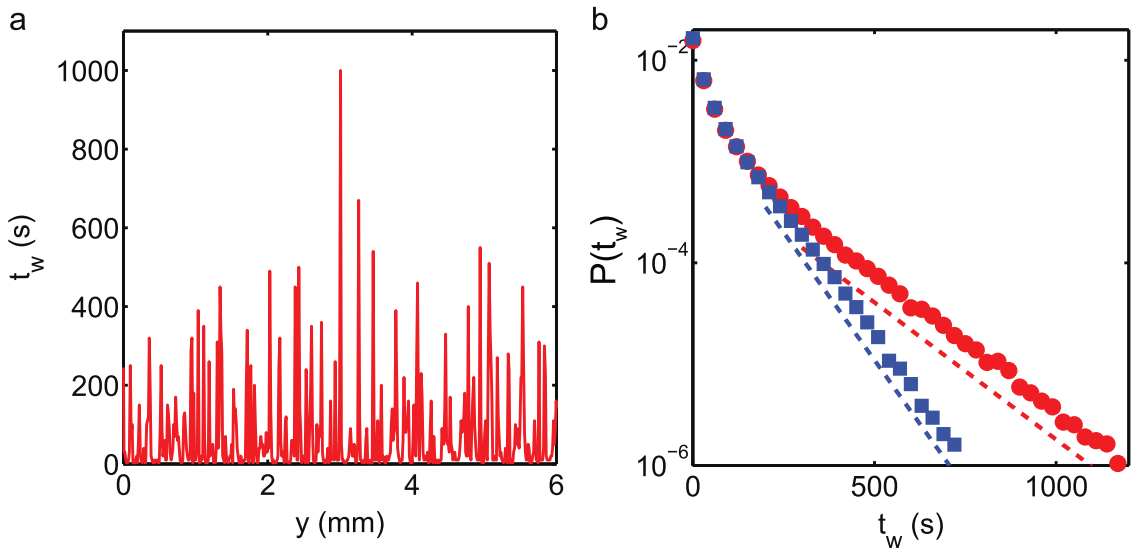

Fig. 6. Analysis of waiting times in the high fracture energy contrast regime. (a) Waiting times as a function of the y coordinate for Exp. 1. The discretization is $\Delta y = 15$ μm. (b) Distribution of waiting times for Exp. 1 Exp. 1 (●) and Exp. 2 (■) along with an exponential fit of the tail (dashed lines). Measured characteristic waiting times are $T_w = 160$ s for Exp. 1 and 90 s for Exp. 2.

Now we consider the waiting time distribution. We measure the time spent by a front at the position y within Δy. Fig. 6 shows an example of the waiting time as a function of y and reflects more accurately the speed distribution at speeds much smaller that v_m since $\Delta y/t_w$ is actually a measure of the front velocity when pinned on defects. The wide distribution of time is revealed more quantitatively by the distributions of waiting times presented in Fig. 6. The distribution shows an exponential tail for large t_w, $P(t_w) \sim \exp(-t_w/T_w)$ where T_w is a characteristic waiting time. We found that $T_w = 160$ s for Exp. 1 and 90 s for Exp. 2 with only a weak dependence on the choice of Δy. Unlike the distribution of displacements, t_w depends strongly on v_m. To match the imposed mean velocity, the jumps characteristic length and typical waiting times should be in such proportion that on average $v_m \sim L_j/T_w$. We measure $L_j/T_w = 0.07$ μm/s for Exp. 1 and 0.1 μm/s for Exp. 2. The agreement with the corresponding mean velocity is off by a factor of 3. However a better agreement is obtained by considering their ratios which is 0.6 and agrees well with the ratio of v_m which is 0.58. Indeed, taking the ratio allows us to cancel out any non-dimensional factors in the relation between v_m, L_j and T_w.

In the high fracture energy contrast regime, we found a clear relation between the microstructure and the dynamics. The crack front dynamics is slaved by the distribution of disorder leading to a kind of stick-slip motion with a well defined characteristic waiting time given by $T_w \sim L_{\|}$. This scaling allows a direct control of the crack growth by tuning the characteristics of the disorder keeping all other parameters such as the material properties constant. Indeed, we can speculate that the dissipation is always significant even at vanishing v_m and a more general loading force because the motion happens by jumps much faster than the average speed, which leads to high dissipation. This study can be compared with recent results showing that the fracture energy of disordered material can be enhanced only in the high fracture energy contrast regime whereas no obvious toughening mechanism was found for low fracture energy contrast (Patinet et al., 2013).

5. Conclusion

We have presented an experimental setup enabling the study of the morphology and the dynamics of a crack front propagating in a disordered interface. Using lithographic techniques, we are able to prescribe the shape and spatial distribution of defects and change the fracture energy contrast allowing us to explore the regimes of high and low fracture energy contrast. In both regimes, the roughness analysis does not reveal any scale invariant properties nor well defined roughness exponents. We identified an intermediate length scale that can be modeled easily considering a single defect. We argue that finite size effects are responsible for an attenuation of fluctuations at a scale much smaller than the system size. Indeed, the proposed cutoff is found to scale as the geometrical mean between the crack length and the typical size of defects. This is agreement with a recent set of studies showing the importance of finite size effects in related systems but in different geometry and dimensionality (Katzav et al., 2007; Katzav and Adda-Bedia, 2013). Our results show explicitly that the morphology of the crack front only provides a limited access to the whole crack dynamics. In our experimental setup, we have access to the instantaneous dynamics which allows to discriminate between high and low fracture energy contrast and draw a clear connection with the characteristics of the disordered pattern. In the high fracture energy contrast regime, we found that the statistics of jumps and waiting time is directly related to the distribution of defects. This tight connection is however lost in the low fracture energy contrast regime where the elastic interaction seems to average out the detailed

feature of the disorder. Future work should consist of tuning the geometrical properties of disordered patterns and to determine their effects on the crack front statistics. Finally, we hope that our results will trigger further numerical and theoretical studies considering situations closer to experiments.

Acknowledgments

We thank Jean-Baptiste Leblond and Eytan Katzav for fruitful discussions concerning the theoretical part of this work and two anonymous referees for their critical and thorough reading and useful comments on the paper.

References

Yang, W., Li, Z.-M., Shi, W., Xie, B.-H., Yang, M.-B., 2004. Review on auxetic materials. J. Mater. Sci. 39 (10), 3269–3279.
Bonn, D., Eggers, J., Indekeu, J., Meunier, J., Rolley, E., 2009. Wetting and spreading. Rev. Mod. Phys. 81, 771.
Geim, A.K., Dubonos, S.V., Grigorieva, I.V., Novoselov, K.S., Zhukov, A.A., Shapoval, S.Y., 2003. Microfabricated adhesive mimicking gecko foot-hair. Nat. Mater. 2, 461.
Chan, E.P., Greiner, C., Arzt, E., Crosby, A.J., 2007. Designing model systems for enhanced adhesion. MRS Bull. 32 (06), 496–503.
Xia, S., Ponson, L., Ravichandran, G., Bhattacharya, K., 2012. Toughening and asymmetry in peeling of heterogeneous adhesives. Phys. Rev. Lett. 108, 196101.
Epstein, A., Wong, T., Belisle, R., Boggs, E., Aizenberg, J., 2012. Liquid-infused structured surfaces with exceptional anti-biofouling performance. Proc. Natl. Acad. Sci. 33, 13182.
Mower, T.M., Argon, A.S., 1995. Experimental investigations of crack trapping in brittle heterogeneities solides. Mech. Mater. 19, 343.
Alexandre, M., Dubois, P., 2000. Polymer-layered silicate nanocomposites: preparation, properties and uses of a new class of materials. Mater. Sci. Eng. R: Rep. 28, 1.
Hull, D., 1999. Fractography. Cambridge University Press, Cambridge.
Suresh, S., 1998. Fatigue of Materials. Cambridge university press, Cambridge.
Lawn, B., 1993. Fracture of Brittle Solids, second ed. Cambridge University Press, Cambridge.
Mandelbrot, B.B., Passoja, D.E., Paullay, A.J., 1984. Fractal character of fracture surfaces of metals. Nature 308, 721.
Bouchaud, E., Lapasset, G., Planès, J., 1990. Fractal dimension of fractured surfaces: a universal value?. Europhys. Lett. 13, 73.
Engoy, T., Måløy, K.J., Hansen, A.J., Roux, S., 1994. Roughness of two-dimensional cracks in wood. Phys. Rev. Lett. 73, 834.
Plouraboué, F., Winkler, K.W., Petitjean, L., Hulin, J.P., Roux, S., 1996. Experimental study of fracture surface roughness on rocks with crack velocity. Phys. Rev. E 53, 277.
Ponson, L., Auradou, H., Pessel, M., Lazarus, V., Hulin, J.P., 2007. Failure mechanisms and surface roughness statistics of fractured fontainebleau sandstone. Phys. Rev. E 76, 036108.
Dalmas, D., Lelarge, A., Vandembroucq, D., 2008. Crack propagation through phase separated glasses: effect of the characteristic size of disorder. Phys. Rev. Lett. 101, 255501.
Bouchaud, E., 1997. Scaling properties of crack. J. Phys. Condens. Matter 9, 4319.
Bonamy, D., Santucci, S., Ponson, L., 2008. Crackling dynamics in material failure as the signature of a self-organized dynamic phase transition. Phys. Rev. Lett. 101 (4), 045501.
Bonamy, D., 2009. Intermittency and roughening in the failure of brittle heterogeneous materials. J. Phys. D: Appl. Phys. 42, 214014.
Schmittbuhl, J., Måløy, K.J., 1997. Direct observation of a self-affine crack propagation. Phys. Rev. Lett. 78 (20), 3888.
Delaplace, A., Schmittbuhl, J., Måløy, K.J., 1999. High resolution description of a crack front in a heterogeneous plexiglas block. Phys. Rev. E 60, 1337.
Santucci, S., Grob, M., Toussaint, R., Schmittbuhl, J., Hansen, A., Måløy, K.J., 2010. Fracture roughness scaling: a case study on planar cracks. Europhys. Lett. 92, 44001.
Gao, H., Rice, J.R., 1989. A first order perturbation analysis of crack trapping by arrays of obstacles. J. Appl. Mech. 56, 828.
Schmittbuhl, J., Roux, S., Vilotte, J.-P., Jorgen Måløy, K., 1995. Interfacial crack pinning: effect of nonlocal interactions. Phys. Rev. Lett. 74, 1787–1790, http://dx.doi.org/10.1103/PhysRevLett.74.1787.
Chopin, J., Prevost, A., Boudaoud, A., Adda-Bedia, M., 2011. Crack front dynamics across a single heterogeneity. Phys. Rev. Lett. 107, 144301.
Dalmas, D., Barthel, E., Vandembroucq, D., 2009. Crack front pinning by design in planar heterogeneous interfaces. J. Mech. Phys. Solids 57 (3), 446–457.
Kardar, M., 1998. Nonequilibrium dynamics of interfaces and lines. Phys. Rep. 301 (1), 85–112.
Roux, S., Vandembroucq, D., Hild, F., 2003. Effective toughness of heterogeneous brittle materials. Eur. J. Mech. A/ Solids 22, 743.
Patinet, S., Vandembroucq, D., Roux, S., 2013. Quantitative prediction of effective toughness at random heterogeneous interfaces. Phys. Rev. Lett. 110, 165507.
Démery, V., Rosso, A., Ponson, L., 2014. From microstructural features to effective toughness in disordered brittle solids. EPL (Europhys. Lett.) 105 (3), 34003.
Adda-Bedia, M., Katzav, E., Vandembroucq, D., 2006. Second-order variation in elastic fields of a tensile planar crack with a curved front. Phys. Rev. E 73, 035106R.
Katzav, E., Adda-Bedia, M., Derrida, B., 2007. Fracture surfaces of heterogeneous materials: a 2d solvable model. EPL (Europhys. Lett.) 78 (4), 46006.
Leblond, J.-B., 2003. Mécanique de la Rupture Fragile et Ductile. Hermes Science Publications, Paris.
Patinet, S., Alzate, L., Barthel, E., Dalmas, D., Vandembroucq, D., Lazarus, V., 2013. Finite size effects on crack front pinning at heterogeneous planar interfaces: experimental, finite elements and perturbation approaches. J. Mech. Phys. Solids 61, 311–324.
Schmittbuhl, J., Vilotte, J., Roux, S., 1995. Reliability of self-affine measurements. Phys. Rev. E 51, 131.
Bakke, J.Ø.H., Hansen, A., 2007. Accuracy of roughness exponent measurement methods. Phys. Rev. E 76, 031136.
Hansen, A.J., Schmittbuhl, J., 2003. Origin of the universal roughness exponent of brittle fracture surfaces: stress-weighted percolation in the damage zone. Phys. Rev. Lett. 90, 045504.
Legrand, L., Patinet, S., Leblond, J.-B., Frelat, J., Lazarus, V., Vandembroucq, D., 2011. Coplanar perturbation of a crack lying on the mid-plane of a plate. Int. J. Fract. 170, 67–82, http://dx.doi.org/10.1007/s10704-011-9603-0.
Måløy, K., Schmittbuhl, J., 2001. Dynamical event during slow crack propagation. Phys. Rev. Lett. 87 (10), 105502.
Tallakstad, K., Toussaint, R., Santucci, S., Schmittbuhl, J., Måløy, K., 2011. Local dynamics of a randomly pinned crack front during creep and forced propagation: an experimental study. Phys. Rev. E 83, 046108.
Katzav, E., Adda-Bedia, M., 2013. Stability and roughness of tensile cracks in disordered materials. Phys. Rev. E 88, 052402.